Kobe University Repository : Kernel

PDF issue: 2025-12-05

Quantitative NMR of quadrupolar nucleus as a novel analytical method: hydrolysis behaviour analysis of aluminum ion

Maki, Hideshi
Sakata, Genki
Mizuhata, Minoru

(Citation)
Analyst,142(10):1790-1799

(Issue Date)
2017-05-21

(Resource Type)
journal article

(Version)
Accepted Manuscript

(Rights)
©2017 Royal Society of Chemistry

(URL)
https://hdl.handle.net/20.500.14094/90004065

KOBE UNIVERSITY

Quantitative NMR of quadrupolar nucleus as a novel analytical method : Hydrolysis behavior analysis of aluminum ion

Hideshi Maki[a,b]*, Genki Sakata[b], Minoru Mizuhata[b]

[a]Center for Environmental Management, Kobe University, 1-1 Rokkodai-cho, Nada-ku, Kobe 657-8501, Japan

[b]Department of Chemical Science and Engineering, Graduate School of Engineering, Kobe University, 1-1 Rokkodai-cho, Nada-ku, Kobe 657-8501, Japan

CORRESPONDING AUTHOR FOOTNOTE

Authors to whom correspondence should be addressed. E-mail: maki@kobe-u.ac.jp

Keywords: ^{27}Al NMR, qNMR, Ferron, Polynuclear complex, Keggin, Hydrolysis

Abstract

In this study, quantitative nuclear magnetic resonance (qNMR) spectroscopy of quadrupolar nuclei has been established. The complicated hydrolysis behavior of the Al^{3+} ion, which causes fish poisoning and inhibits the growth of plants in environmental water, was clarified by ^{27}Al qNMR spectroscopy. Highly accurate simultaneous multicomponent quantitative analysis of various hydrolyzed forms of the Al ion was achieved in a non-destructive manner. The calibration curve of the external standard aqueous $Al(NO_3)_3$ solution showed excellent linearity over a very wide concentration range from 1×10^{-4} to 1 mol L^{-1} (an increase in concentration of 10000 times), with a simple experimental and analytical procedure. Furthermore, the weaknesses of the conventional Ferron assay and the advantages of ^{27}Al qNMR spectroscopy were considered. The quantitative determination error

for the free $[Al(H_2O)_6]^{3+}$ ion and the trinuclear complex, which has a high complexation rate, is higher in the Ferron assay than in the ^{27}Al qNMR technique. The concentrations of four Al species were directly determined by ^{27}Al qNMR, namely, free $[Al(H_2O)_6]^{3+}$, the trinuclear complex, $Al(OH)_4^-$, and tridecameric hydrolyzed Al, which has a Keggin structure. The concentration of the tridecamer rapidly increased until 100 min after NaOH addition, and showed a local maximum after 1 week. In addition, the concentration of colloidal Al hydroxide, which cannot be detected by NMR spectroscopy, was determined by numerical analysis. This species was generated in the initial stage of reaction, and then the tridecamer formed very slowly.

1. Introduction

It has recently been reported that Al causes fish poisoning and inhibits the growth of plants.[1] Moreover, ingestion of large amounts of Al has adverse effects on the kidneys and bladder of mammals.[1,2] It is therefore important to control the use of Al-containing food additives and decrease the Al concentration in environmental water. One effective way of reducing the Al concentration in environmental water is by decreasing the use of polyaluminum chlorides (PACs), which are precipitants used in sewage disposal.[2,3] To do this, it is necessary to quantify the hydrolysis behavior of the Al^{3+} ion in aqueous solution.

Hydrolysis of the Al^{3+} ion has previously been investigated by NMR spectroscopy, time-of-flight mass spectrometry (TOF-MS),[4,5] X-ray photoelectron spectroscopy (XPS),[6] and small angle X-ray scattering (SAXS).[7] The Al^{3+} ion exhibits extremely complicated hydrolysis behavior in aqueous solution; this behavior depends, among others, on the Al concentration, pH, and temperature.[4–16] Furthermore, the formation of various dissolved Al complexes, such as free $[Al(H_2O)_6]^{3+}$ (Al_1), the Al dimer (Al_2), the Al trimer (Al_3), the Al tridecamer (Al_{13}), and the Al triacontamer (Al_{30}), and the precipitation of Al hydroxides have been confirmed.[4,5,10,12–16] However, the hydrolysis behavior of the

Al^{3+} ion has not yet been quantified because destructive measurement methods were used for the analysis.

Frequently used non-destructive analysis methods include absorptiometric methods, such as the Ferron method.[3,14,15,17] The Ferron method uses numerical analysis of the formation behavior of various dissolved Al species based on the time dependence of Al–Ferron complex formation. Hence, it is difficult to accurately determine the extremely complicated hydrolysis behavior of the Al^{3+} ion using the Ferron method. In contrast, non-destructive multicomponent simultaneous quantitative analysis of the dissolved species can be directly facilitated by NMR spectroscopy.[18–20] NMR spectroscopy uses a low-energy electromagnetic wave, which means that the energy perturbation of the observed system is extremely small. Therefore, in situ and in vivo analyses of systems involving various reactions, equilibria, and intermolecular interactions are possible with NMR spectroscopy.

Until recently, NMR spectroscopy was considered to be inferior to other analysis methods from the point of view of quantitative accuracy. However, the quantitative accuracy of NMR analysis has improved rapidly in recent years, and quantitative accuracy of three significant figures (with errors of 0.5% or less) is now possible. As a result, high-accuracy quantitative NMR (qNMR) analysis can be achieved while retaining the advantages of NMR spectroscopy,[18–28] such as its non-destructive nature and simultaneous multicomponent analysis. Previously, assuming that all of the observable nuclei were detected, the concentrations of specific chemical species and functional groups in the measured sample could be determined from the relative intensities of each NMR signal. In contrast, the concentration of a specific chemical species or functional group can be directly determined by qNMR from the integrated intensity of the corresponding NMR signal if a known amount of an internal standard is added and a calibration curve is prepared with an external standard. All nuclei can be classified as dipolar or quadrupolar nuclei in terms of magnetic resonance; dipolar nuclei (e.g., ^{1}H, ^{13}C, ^{19}F, ^{29}Si, and ^{31}P) have a spin quantum number of 1/2 and quadrupolar nuclei (e.g., ^{7}Li, ^{11}B, ^{23}Na, ^{27}Al, and ^{35}Cl) have a spin quantum number that is not 1/2. qNMR analysis has been reported for many dipolar

nuclei.[18–28] However, qNMR spectroscopy of quadrupolar nuclei, which includes that of many metallic nuclei, has not yet been reported because of the fundamental differences in the governing factors of the nuclear magnetic relaxation process for quadrupolar and dipolar nuclei.

Previously, Gerardin et al. quantified the hydrolysis and condensation of Al using variable-temperature ^{27}Al NMR spectroscopy.[29] They evaluated the dependence of the NMR signal intensity on the Al concentration, temperature, pH, and ionic strength. However, the calibration curve obtained with the external standard solution was curved and required a complicated correction using the quality factor (Q factor) of the probe. Furthermore, the linearity of the corrected calibration curve was low, and the applicable Al concentration range was narrow, only 0.01–0.80 mol L^{-1}. A calibration curve with high linearity and a wide dynamic range that is comparable to those of existing spectroscopies [e.g., atomic absorption spectroscopy (AAS) and inductively coupled plasma-optical emission spectrometry (ICP-OES)] is essential for qNMR spectroscopy of quadrupolar nuclei to be accepted as a quantitative analytical tool. Moreover, this calibration curve should be achieved through a simple experimental and analytical procedure.

In this work, highly accurate simultaneous multicomponent quantitative analysis of various dissolved Al species was achieved using a non-destructive and simple ^{27}Al qNMR technique, and the complicated hydrolysis behavior of the Al^{3+} ion was clarified. This technique extends the qNMR method to quadrupolar nuclei, and enables the simple, non-destructive and simultaneous multicomponent quantitative analysis of complicated systems involving complex formation. The new method will also make it possible to clarify the dissolution state of various metal ions and anions by qNMR spectroscopy of quadrupolar nuclei.

2. Experimental

2.1. Preparation of measurement solutions for ^{27}Al qNMR calibration curve

All chemicals used in this work were of analytical grade and were purchased from Nacalai Tesque Inc. The $Al(NO_3)_3$ aqueous solutions of 1×10^{-4} – 1 mol L^{-1} which contain 0.10 mol L^{-1} HNO_3 were employed as standard solutions for ^{27}Al qNMR calibration curve. The total concentrations of Al^{3+} ion in the standard solutions were exactly determined by an ICP-OES (HORIBA Ltd., ULTIMA 2000). Measurement solutions for the observation of Al^{3+} ion hydrolysis behavior were prepared by the mixture of $AlCl_3$ and NaOH aqueous solutions.

2.2. ^{27}Al qNMR measurements

All NMR spectra were recorded on a Varian INOVA 400 (9.39 T) pulse FT-NMR spectrometer with a tunable broad-band probe at room temperature. ^{27}Al NMR spectra were recorded at an operating frequency of 104.218 MHz, and were applied a sweep width of 39.999 kHz (383.804 ppm); the data acquisition time was 1.0 s, and the data number during the free induction decay (i.e., FID) were collected in 40000 points; *i.e.*, the resolution of the spectra on a frequency region was 1.000 Hz (0.009595 ppm). The Lorentzian line-broadening factor of 1.0 Hz was applied to the total FID prior to Fourier transformation. Scans of 4 - 4096 times were recorded without recycle delay (i.e., the recycle delay is 0 s) between 30° pulse sequences which pulse width is 8.5 μs to improve the signal-to-noise ratio and to avoid saturation. The very short time lag between the pulse irradiation and the FID acquisition start (i.e., dead time) was set for 5 ms. It was confirmed that the application of the relaxation delay and the dead time did not change the intensity of ^{27}Al NMR spectra. The receiver gain of a RF amplifier in an NMR spectrometer was normally set to 60 dB. When the receiver gain was changed, it clearly described in the text. All ^{27}Al NMR measurements were carried out at 30 ˚C. The temperature of the sample solution was calibrated by 1,2-ethanediol with Van Geet's method.,[30,31] whose accuracy was ± 1.0 °C or better, and the reproducibility was lower than 0.2 °C. To avoid the contamination of D_2O for the field-frequency locking into the sample solutions, the coaxial NMR tube system was employed for the all NMR measurements in this work. The coaxial NMR tube system

consists of a borosilicate inner (516-I-5, Wilmad-LabGlass) and outer (516-CC-5, Wilmad-LabGlass) NMR tubes. Outside diameter and inside diameter of the outer tube are 5.00 mm and 3.97 mm respectively, and those of the inner tube are 3.97 mm and 2.97 mm, respectively. A proper quantity of the measurement solutions were put into the inner tube in the outer tube which a small amount of D_2O was put into as shown in Scheme S1(Supporting Information). The ^{27}Al NMR chemical shifts were determined against an external standard of 0.10 mol L^{-1} $Al(NO_3)_3$ + 0.10 mol L^{-1} HNO_3 in 10 % D_2O for 0 ppm. The discreet phase corrections were performed before the calculations of the integrated intensities of ^{27}Al NMR signals of all the measurement solutions, thus it can be concluded that ^{27}Al NMR peak area was nearly proportional to the number of ^{27}Al nuclei producing the NMR resonance.

2.3. Presumption of the formation behavior of Al dissolved species by Ferron method

All sample solutions of PAC were prepared as follows (see Scheme S2 in the Supporting Information). The appropriate amount of aqueous NaOH solution (0.1, 0.5, or 1.0 mol L^{-1}) was added at a rate of 1 mL min^{-1} with an automatic piston burette (APB-510, Kyoto Electronics Manufacturing Co., Ltd.) to 4 mL of an aqueous $AlCl_3$ solution of the same concentration in a 40-mL volumetric flask. The solutions were then aged for 1 week at 30 °C. The total concentrations of Al and NaOH were determined before aging by ICP-OES (ULTIMA 2000, Horiba Ltd.) and neutralization titrations, respectively. The OH/Al ratio indicates the molar ratio of added NaOH and $AlCl_3$, and the range of OH/Al ratios was 0–9.

The Ferron assay was carried out as follows[14] (see Scheme S3 in the Supporting Information). The Ferron colorimetric solution was prepared by mixing 0.2% (w/v) aqueous 8-hydroxy-7-iodo-5-quinoline-sulfonic acid (Ferron), 20% (w/v) aqueous CH_3COONa, and 3.5% (v/v) aqueous HCl in a ratio of 5:4:2 (v/v/v). The Ferron colorimetric solution (5.5 mL) was placed in 40-mL volumetric flasks, and then PAC sample solutions with total Al concentrations (C_{Al}) of 0.01 (20 μL), 0.05 (100 μL), and 0.10 mol L^{-1} (200 μL) (i.e., the molar ratio of Ferron and Al was kept constant at 25) were added with a

micro-syringe. The reaction start time was recorded on addition of the PAC sample solution. After sufficient mixing, the reacting sample solution was quickly transferred to a 1-cm quartz cell. The absorbance changes at 366 nm were monitored automatically by recording the UV-Vis spectra (V-7200, Jasco Corp.) every second from a reaction time of 60 s to 2 h. Determination of the concentrations of the various Al complexes by numerical analysis of the time dependence of the absorbance was carried out as previously reported by W. Zhou et al.[17]

3. Results and discussion

3.1. Evaluation of the experimental parameters affecting the accuracy and precision of ^{27}Al qNMR.

When qNMR is carried out, the proportionality between the integrated intensity of the NMR signals and the number of nuclei should be carefully confirmed.[18] Fig. 1 shows the relationship between the integrated intensity of the ^{27}Al NMR signals per FID scan and the concentration of free Al^{3+} ions (i.e., $[Al(H_2O)_6]^{3+}$) for aqueous solutions of $Al(NO_3)_3$, which is an external reference solution for ^{27}Al qNMR. All of the raw data are listed in Table S1 (Supporting Information). The obtained ^{27}Al NMR spectra consist of a singlet assigned to the $[Al(H_2O)_6]^{3+}$ ion. Careful phase correction is necessary because errors in phase correction result in a decrease in the integrated intensities of the NMR signals.[32] The integrated intensities were calculated in the frequency range of five times the peak width at half height of the signals. Theoretically, the proportional relationship between the integrated intensity of signal I_x and the number of nuclei, that is, the concentration of chemical species C_x[33] is confirmed as follows:

$$I_x = \text{slope} \times C_x \quad (1)$$

Taking the logarithm of both sides allows us to verify the above-mentioned relationship over a wide concentration range:

$$\log (I_x) = \log (\text{slope}) + \log (C_x) \quad (2)$$

The results of the linear approximation by the linear least squares procedure using Eqs. 1 and 2 are shown in Table 1. There is extremely good linearity in the very wide concentration range from 1×10^{-4} to 1 mol L^{-1} (an increase in concentration of 10000 times) for both the real number axis plot [Fig. 1(a)] and the logarithmic axis plot [Fig. 1(b)]. The equivalent concentration ranges for other spectroscopic methods (e.g., AAS, UV-Vis, and ICP-OES) are very narrow. The very large concentration range thus indicates that qNMR analysis is possible for this system.

Identifying the NMR parameter that determines the relationship between the integrated intensity and the concentration of the chemical species is useful for assessing the practicability of qNMR spectroscopy. When an external standard is used, the following relationship is theoretically established between the integrated intensity of the NMR signal and the concentration of the chemical species dissolved in the external standard solution:[18]

$$\frac{C_x}{C_{ref}} = A \times 10^{\frac{Rg_{ref} - Rg_x}{20}} \times \frac{N_{ref}}{N_x} \times \frac{I_x}{I_{ref}} \quad (3)$$

where C is the concentration of the chemical species that gives the NMR signal, Rg is the gain of the radio frequency amplifier in the NMR spectrometer (the receiver gain), N is the number of FID scans, and I is the integrated intensity of the NMR signal. The subscripts ref and x represent the external standard solution and the sample solution, respectively. A is a specific constant for the measurement system including the NMR sample tube and the entire NMR equipment, and it is almost equal to 1

when a similar NMR sample tube and the same NMR equipment are used for measurements of both the external standard and sample solution. In this study, the influence of the number of FID scans and the receiver gain on the accuracy of the ^{27}Al qNMR technique was evaluated, and the results are shown in Fig. 2(a) and 2(b), respectively. All of the raw data are listed in Table S2 (Supporting Information). The results of a linear approximation using the linear least squares procedure are shown in Table 2 and confirm the extremely good linear relationships between the integrated intensity of the NMR signal and the number of FID scans, and the integrated intensity and the receiver gain. This demonstrates that the reproducibility and accuracy of the pulse generator and radio frequency transmitter, and the linearity of the RF amplifier in the NMR equipment are excellent. The influence of the FID acquisition time on the integrated intensity is shown in Fig. 2(c). The FID data cannot be fully obtained when the FID acquisition time is too short, and, as a result, the integrated intensity decreases. However, the NMR measurement time increases if the FID acquisition time is too long, so an appropriate setting is desirable. In this study, the integrated intensity of the NMR signal was almost constant for FID acquisition times of greater than 0.8 s, as shown in Fig. 2(c). The above results thus show that it is possible to perform ^{27}Al qNMR spectroscopy with high accuracy and short measurement times.

The temperature of the sample solution also affects the integrated intensity of the NMR signal. There are two main reasons for this. First, expansion of the solution volume with increasing temperature causes a decrease in the integrated intensity. The second reason concerns the principle of magnetic resonance. When a nucleus is placed in a magnetic field, it takes different spin states with different energies. The *z* components of the magnetic moments of the nuclei in the higher energy state are cancelled by those of nuclei in the lower energy state, so only a small excess in the lower energy state gives rise to an observable magnetic resonance effect. When the Boltzmann distribution is applied to a nuclear spin system with different energies, the following relationship can be established:[34]

$$\frac{N_H}{N_L} = \exp\left(\frac{-\Delta E}{kT}\right) \quad (4)$$

where N_H and N_L are the numbers of nuclei in the higher and lower energy states, respectively, ΔE is the energy separation between the higher and lower energy states, k is the Boltzmann constant, and T is the absolute temperature. An increase in the temperature of the sample solution causes a decrease in N_H/N_L, and a consequent decrease in the observable magnetic resonance effect (the integrated intensity of the NMR signal). The dependence of the relationship between the integrated intensity of the ^{27}Al NMR signal originating from the $[Al(H_2O)_6]^{3+}$ ion and the concentration of this ion on the temperature of the sample solution is shown in Fig. 3, and all of the raw data are listed in Table S3. Furthermore, the results of the linear approximation using the linear least squares procedure (Eq. 2) are shown in Table 3. As mentioned above, both the slopes and intercepts of the linear approximation lines decrease with increasing temperature of the sample solution. Notably, an extremely good linear relationship was achieved over a very wide concentration range for all measured temperatures.

The Al^{3+} ion has a large positive charge and a small ionic radius. It has a high positive charge/ionic radius ratio of 6.0 $Å^{-1}$, which means that a high density of positive charge exists around the Al nucleus, and that the Al^{3+} ion can form an ion pair and interact with counteranions. The extremely high energy resolution of NMR spectroscopy makes it likely that an interaction between the Al^{3+} ion and a counteranion will perturb the NMR signal strength. It is therefore useful to evaluate the influence of the counteranion on the integrated intensity of the NMR signal. Fig. S1 shows the influence of the counteranion on the dependence of the integrated intensity of the $[Al(H_2O)_6]^{3+}$ signal on the irradiation pulse width. It is clear that the dependence on the irradiation pulse width is almost the same for all counteranion species. This indicates the high accuracy and versatility of the ^{27}Al qNMR method.

3.2. Comparison between the ^{27}Al qNMR analysis and the Ferron assay.

Absorptiometric methods, such as the Ferron assay, are often used to analyze the hydrolysis behavior of Al in aqueous solution.[3,14,15,17] The Ferron assay is used to determine the concentration distribution of various Al species by numerical analysis of the time dependence of Al–Ferron complex formation. However, the Ferron assay has the following disadvantages:

1. It cannot sufficiently trace the hydrolysis behavior of the Al^{3+} ion because the method is limited to acidic conditions of pH ≤ 5.
2. It results in errors in the concentration of the free $[Al(H_2O)_6]^{3+}$ ion, the main chemical species present immediately after the start of the experiment, because some time is required to perform the experiment.
3. Tracing the hydrolysis behavior immediately after the start of the Al^{3+} hydrolysis reaction is not possible because several hours are required to complete the experiment owing to the slow rate of Al–Ferron complexation.
4. The solid phase that exists in the reaction mixture markedly decreases the absorbance of the solution because of the Tyndall phenomenon. Hence, in absorptiometric analysis methods, it is, in fact, impossible to observe a heterogeneous system containing a solid phase.

Most other spectroscopic methods, such as ICP-OES and TOF-MS, are destructive, so they are not suitable for tracing complexation equilibria. In contrast, NMR spectroscopy has the following advantages:

1. It is a non-destructive method, and the perturbation (i.e., the influence of the energy) on the observed chemical system is extremely small. Therefore, in situ analysis of reacting chemical systems is possible when the free energy change of the reaction is small and the reaction rate is slow, as is the case for hydrolysis of the Al^{3+} ion.

2. There is high linearity between the concentration of the chemical species and the integrated intensity of the NMR signal, as discussed in Section 3.1. As a result, it is possible not only to trace chemical reactions, but also to determine chemical equilibrium constants.[35–39] Furthermore, variable temperature measurements allow analysis of the reaction rate and determination of the activation energy.

3. It has an extremely high ability to distinguish chemical species. Therefore, the simultaneous, multicomponent determination of very different chemical species formed by complicated complexation and hydrolysis reactions is possible. In particular, the Al^{3+} ion has the lowest ligand exchange rate among all metal ions, and this exchange rate is slower than the NMR timescale. As a result, the ^{27}Al NMR signals are not homogenized, and it is possible to resolve separate signals that correspond to different chemical species, such as very different complexes and hydrolysis species.

4. In principle, the existence of a solid phase does not prevent the observation of the solution NMR spectrum. This means that the NMR technique is suitable for in situ analysis of a wide variety of systems in which solids and liquids coexist, not only for studying the hydrolysis of metal ions.

On the basis of the above discussion, the dependence of the ^{27}Al NMR spectra of aqueous PAC solutions aged for 1 week on the OH/Al concentration ratio (i.e., the ratio of added NaOH to the total amount of $AlCl_3$) was determined at 30 °C to elucidate the hydrolysis behavior of the Al^{3+} ion, as shown in Fig. 4. The NMR spectrum contained three main signals for all total concentrations of Al^{3+} ions. The two singlets at 0 and 80 ppm are reported to originate from the $[Al(H_2O)_6]^{3+}$ and aluminate $[Al(OH)_4^-]$ ions, respectively,[5,6,9,10,16] whereas the singlet at 62.5 ppm is from tridecameric hydrolyzed Al $[AlO_4Al_{12}(OH)_{24}(H_2O)_{12}^{7+}$, K-$Al_{13}]$, which has a Keggin structure.[5,6,9,10,14–16] K-Al_{13} contains a central Al atom that is coordinated to four O atoms and surrounded by 12 Al atoms, which are octahedrally coordinated and linked by OH bridges to the O atoms coordinated to the central Al atom. The four-coordinate central Al atom is in a high symmetry environment and gives a narrow ^{27}Al NMR signal at 62.5 ppm.[6,9,10,14,15] In contrast, the octahedral Al atoms are in highly distorted environments

and the NMR quadrupole relaxation efficiency is extremely high. As a result, the ^{27}Al NMR signal corresponding to these atoms has an extremely broad linewidth and is not usually observed.[9,10,14] The weak singlet observed at slightly lower magnetic field (4.0 ppm) than the singlet from the $[Al(H_2O)_6]^{3+}$ ion, shown in the enlarged spectrum in Fig. 4, originates from the Al trimer (Al_3).[5] The ^{27}Al spin–lattice (T_1) and spin–spin relaxation times (T_2) of all Al species were determined by the inversion recovery[40,41] and Carr-Purcell-Meiboom-Gill (i.e.,CPMG) procedures,[42-44] as shown in Table S4. This confirmed that T_1 and T_2 were much shorter than the FID acquisition time, and therefore, that ^{27}Al spin–lattice and spin–spin relaxation is almost complete ahead of the pulse radiation. The dependence of the distribution of the various Al complexes on the OH/Al ratio was calculated for aqueous PAC solutions aged for 1 week at 30 °C on the basis of the assignment of the ^{27}Al qNMR signals and the calibration curve (Fig. 1), as shown in Fig. 5 (top). The dependence on the OH/Al ratio calculated from a traditional Ferron assay of aqueous PAC solutions is also shown in Fig. 5 (bottom). As mentioned above, the only Al atom in the K-Al_{13} complex that can be observed by ^{27}Al qNMR spectroscopy is the four-coordinate central Al atom (Al_{IV}). Therefore, the total Al concentration that corresponds to the K-Al_{13} species is the concentration obtained by ^{27}Al qNMR spectroscopy multiplied by 13.[14,15]

We identified a difference between the total concentration of added Al and the total concentration of all Al species determined by ^{27}Al qNMR analysis for OH/Al ratios of 2.5–4.0. This can be explained by the generation of a colloidal polynuclear Al oligomer (Al_{col}). The ^{27}Al nuclei in the Al_{col} species are in highly distorted, low symmetry environments, and the molecular mobility is limited. These nuclei therefore have a relatively rapid quadrupole relaxation rate, which means their ^{27}Al NMR resonances have an extremely broad linewidth and the signals are not observed. In conventional NMR analysis, the concentration of the chemical species and functional groups in a solution is determined from the relative integrated intensities of the NMR signals, assuming that all observable nuclei in the solution are detected. However, the disadvantage of conventional NMR analysis is the large error in the quantitative accuracy of the concentrations of all chemical species when a species such as Al_{col} is

present in the solution. In contrast, in qNMR analysis, the presence of a chemical species that cannot be detected by NMR spectroscopy does not influence the quantitative accuracy in determining the concentrations of the other chemical species because the concentrations are directly determined by a separately prepared calibration curve. Furthermore, even undetectable nuclei can be quantified by qNMR spectroscopy from the difference in the total amount of added nuclei and the total amount detected by NMR spectroscopy. In this study, the total Al concentration in the Al_{col} species (C_{Alcol}) was determined as follows:

$$C_{Alcol} = C_{Al} - C_{[Al(H2O)6]3+} - C_{Al(OH)4-} - C_{Al3} - C_{K\text{-}Al13} \quad (5)$$

where C_{Al3} and $C_{K\text{-}Al13}$ are the total Al concentrations in the Al_3 and K-Al_{13} species, respectively. Comparison of the experimental ^{27}Al qNMR results with those of the Ferron assay (Fig. 5) show a distinct difference between the concentrations of the $[Al(H_2O)_6]^{3+}$ and Al_3 species determined with the two experimental approaches. This result clearly shows that there is an experimental error in the Ferron assay, which arises from the need to determine the concentrations of the relatively low molecular weight $[Al(H_2O)_6]^{3+}$ and Al_3 species in a short time period immediately after the start of the experiment. Moreover, because the hydrolysis progresses quickly and the change in the absorbance is large immediately after the start of the experiment, the experimental error in the Ferron assay increases. In contrast, the concentrations of K-Al_{13}, $Al(OH)_4^-$, and Al_{col} determined by ^{27}Al qNMR spectroscopy and the Ferron assay are in good agreement, which confirms the accuracy and validity of the ^{27}Al qNMR analysis. Furthermore, with ^{27}Al qNMR spectroscopy, it was possible to analyze the hydrolysis behavior of the Al^{3+} ion in a more alkaline region (higher OH/Al ratio) than with the Ferron assay, which suggests the high generalizability of the ^{27}Al qNMR analysis. The time course of the absorbance of the aqueous PAC solutions aged for 1 week at 30 °C determined by the Ferron assay is shown in Fig.

S2, and the fitting parameters and reaction rate constants calculated using the non-linear least squares curve fitting method are shown in Table S5.

3.3. Quantitative evaluation of the temporal change of the hydrolysis equilibrium of PAC.

Finally, we quantitatively evaluated the temporal changes in the hydrolysis equilibrium of PAC by ^{27}Al qNMR. PAC is used as a coagulant in the sewage disposal process, and this evaluation will offer insight into improving the functionality of this process. It will thus help to decrease the Al concentration in environmental water by decreasing the amount of PAC used.

Fig. 6 shows the dependence of the pH of the sample solution on time and the distribution of various hydrolyzed species of Al, as determined by ^{27}Al qNMR of aqueous PAC solutions at 30 °C. The rate of formation of the Al–Ferron complex is slow, and several hours were required to complete the experiments. Hence, observation of the changes that occur within about 100 min of the start of the hydrolysis reaction is not possible using the Ferron assay. However, it should be noted that the ^{27}Al qNMR experiments showed that the concentrations of the various hydrolyzed species of Al change dramatically within this time period. When OH/Al was 1 or 2, the concentration of the large amount of Al_{col} generated immediately after the start of the hydrolysis decreased rapidly in the first 100 min. Moreover, the concentration of K-Al_{13} increased rapidly in the first 100 min, and then increased gradually for several weeks afterwards. This decrease in the Al_{col} concentration and increase in the K-Al_{13} concentration are complementary, that is, it can be considered that Al_{col} forms immediately after initiation of the reaction and K-Al_{13} then forms very slowly from Al_{col}. A local maximum in the concentration of K-Al_{13} was observed after about 1 week, and this species almost completely decomposed into Al_{col} after approximately 6 months. The change in the pH of the reaction solution was extremely small during the same 6 months period. However, when OH/Al was 3.5, the concentration of the $Al(OH)_4^-$ species gradually decreased. This species disappeared completely after approximately 6

months and a gelatinous white precipitate formed. Because the pH of the reaction solution increased, it can be concluded that the white precipitate was $Al(OH)_3$.

$$Al(OH)_4^- + H_2O \rightleftarrows Al(OH)_3 + OH^- \quad (6)$$

4. Conclusions

In this study, qNMR for quadrupolar nuclei was established. Highly accurate simultaneous multicomponent quantitative analysis of various hydrolyzed species of the Al^{3+} ion was achieved in a non-destructive and simple manner with ^{27}Al qNMR, and the complicated hydrolysis behavior of the Al^{3+} ion was clarified. The effects of various experimental parameters, namely, the number of FID scans, receiver gain of the RF amplifier, FID acquisition time, anion species, and temperature, on the accuracy and precision of the ^{27}Al qNMR technique were carefully evaluated. The calibration curve of an external standard, aqueous $Al(NO_3)_3$, showed excellent linearity over a very wide concentration range of 1×10^{-4} to 1 mol L^{-1} (an increase in concentration of 10000 times), and the experimental and analytical procedures were simple. The concentrations of free $[Al(H_2O)_6]^{3+}$, the trinuclear complex, $Al(OH)_4^-$, and K-Al_{13} were directly and accurately determined by ^{27}Al qNMR spectroscopy. Moreover, the concentration of Al_{col}, which cannot be detected by NMR spectroscopy, was determined by numerical analysis. The ^{27}Al qNMR technique is also suitable for analyzing the hydrolysis behavior of the Al^{3+} ion in a more alkaline region than the Ferron assay. The quantitative determination error for the free $[Al(H_2O)_6]^{3+}$ ion and trinuclear complex, which has a high complexation rate, was higher in the Ferron assay than in the ^{27}Al qNMR technique. The concentrations of Al_{col} and K-Al_{13} rapidly decreased and increased, respectively, in the first 100 min of the reaction, and these changes were complementary. Therefore, Al_{col} forms immediately after initiation of the reaction and K-Al_{13} forms from Al_{col}. It is not possible to observe this with the Ferron assay because of the slow formation rate of the Al–Ferron complex. This study thus provides a simple method for the non-destructive simultaneous

multicomponent quantitative analysis of complicated systems that involve complex formation by extending qNMR spectroscopy to quadrupolar nuclei. Furthermore, it will become possible to clarify the dissolution states of metal ions and anions containing quadrupolar nuclei by qNMR spectroscopy.

References

1 B. Fairman and A. Sanz-Medel, *Tech. Instrum. Anal. Chem.*, 1995, **17**, 215-233.

2 Y. X. Zhao, S. Phuntsho, B. Y. Gao, X. Huang, Q. B. Qi, Q. Y. Yue, Y. Wang, J.-H. Kim and H. K. Shon, *Environ. Sci. Technol.*, 2013, **47**, 12966–12975.

3 X. Wu, D. Wang, X. Ge and H. Tang, *Colloids Surf. A*, 2008, **330**, 72–79.

4 C. Feng, Z. Bi and H. Tang, *Environ. Sci. Technol.*, 2015, **49**, 474–480.

5 H. Tang, F. Xiao and D. Wang, *Adv. Colloid Interface Sci.*, 2015, **226**, 78–85.

6 J. L. Lin, C. Huang, B. Dempsey and J. Y. Hu, *Water Res.*, 2014, **56**, 314–324.

7 J. Y. Bottero, D. Tchoubar, M. A. V. Axelos, P. Quienne and F. Fiessinger, *Langmuir*, 1990, **6**, 596–602.

8 J.; Duan and J. Gregory, *Adv. Colloid Interface Sci.*, 2003, **100–102**, 475–502.

9 K. E. Lee, N. Morad, T. T. Teng and B. T. Poh, *Chem. Eng. J.*, 2012, **203**, 370–386.

10 J. W. Akitt, *Prog. Nucl. Magn. Reson. Spectrosc.*, 1989, **21**, 1–149.

11 B. S. Lartiges, J. Y. Bottero, L. S. Derrendinger, B. Humbert, P. Tekely and H. Suty, *Langmuir*, 1997, **13**, 147–152.

12 M. Nofz, J. Pauli, M. Dressler, C. Jäger and W. Altenburg, *J. Sol-Gel Sci. Technol.*, 2006, **38**, 25–35.

13 K. Shafran, O. Deschaume and C. C. Perry, *Adv. Eng. Mater.*, 2004, **6**, 836–839.

14 Y. Changqing, W. Dongsheng, W. Xiaohong and Q. Jiuhui, *J. Colloid Interface Sci.*, 2009, **335**, 44–49.

15 C. Feng, H. Tang and D. Wang, *Colloids Surf. A*, 2007, **305**, 76–82.

16 S. Bi, C. Wang, Q. Cao and C. Zhang, *Coord. Chem. Rev.*, 2004, **248**, 441–455.

17 W. Zhou, B. Gao, Q. Yue and Y. Wang, *Colloids Surf. A*, 2006, **278**, 235–240.

18 H. Maki, Y. Okumura, H. Ikuta and M. Mizuhata, *J. Phys. Chem. C*, 2014, **118**, 11964–11974.

19 G. F. Pauli, B. U. Jaki and D. C. Lankin, *J. Nat. Prod.*, 2005, **68**, 133–149.

20 F.; Malz and H. J. Jancke, *Pharm. Biomed. Anal.*, 2005, **38**, 813–823.

21 U. Brinkmann-Trettenes, P. C. Stein, B. Klösgen and A. J. Bauer-Brandl, *Pharmaceut. Biomed.*, 2012, **70**, 708-712.

22 E. Szłyk and P. Hrynczyszyn, *Talanta*, 2011, **84**, 199-203.

23 D. S. Argyropoulos, H. Li, A. R. Gaspar, K. Smith, L. A. Lucia and O. J. Rojas, *BioOrgan. Med. Chem.*, 2006, **14**, 4017-4028.

24 S. K. Bharti and R. Roy, *Trends Anal. Chem.*, 2012, **35**, 5-26.

25 G. F. Pauli, B. U. Jaki and D. C. Lankin, *J. Nat. Prod.*, 2005, **68**, 133-149.

26 G. F. Pauli, T. Gödecke, B. U. Jaki and D. C. Lankin, *J. Nat. Prod.*, 2012, **75**, 834-851.

27 U. Holzgrade, *Prog. Nucl. Mag. Res. Sp.*, 2010, **57**, 229-240.

28 P. Giraudeau, I. Tea, G. S. Remaud and S. Akoka, *J. Pharmaceut. Biomed.*, 2014, **93**, 3-16.

29 C. Gerardin, M. Haouas, C. Lorentz, F. Taulelle, *Magn. Reson. Chem.*, 2000, **38**, 429-435.

30 A. L. Van Geet, *Anal. Chem.*, 1968, **40**, 2227-2229.

31 S. Braun, H.-O. Kalinowski and S. Berger, *150 and More Basic NMR Experiments: a practical course*, Wiley-VCH, Weinheim, 1998, ch. 5.2.

32 A. E. Derome, *Modern NMR Techniques for Chemistry Research*, Pergamon Press Ltd., Oxford, 1987, ch. 7.6.

33 J. W. Akitt, *NMR and Chemistry: An Introduction to Modern NMR Spectroscopy*, Chapman & Hall, London, 3rd edn, 1992, ch. 5.3.

34 J. W. Akitt, *NMR and Chemistry: An Introduction to Modern NMR Spectroscopy*, Chapman & Hall, London, 3rd edn, 1992, ch. 1.3.

35 H. Maki, K. Ryoushi, H. Nariai and M. Mizuhata, *Dalton. Trans.*, 2014, **43**, 11611-11623.

36 H. Maki, M. Tsujito, H. Nariai and M. Mizuhata, *Magn. Reson. Chem.*, 2014, **52**, 69-81.

37 H. Maki, M. Tsujito and T. Yamada *J. Solution Chem.*, 2013, **42**, 1063-1074.

38 H. Maki, Y. Ueda and H. Nariai. *J. Phys. Chem.*, 2011, **115**, 3571-3577.

39 H. Maki, H. Nariai and T. Miyajima, *Polyhedron*, 2011, **30**, 903-912.

40 R. L. Vold, J. S. Waugh, M. P. Klein and D. E. Phelps, *J. Chem. Phys.*, 1968, **48**, 3831–3832.

41 S. Braun, H. -O. Kalinowski, S. Berger, *150 and More Basic NMR Experiments: a practical course*, WILEY-VCH, Weinheim, 1998, ch. 6.1.

42 S. Meiboom, D. Gill, *Rev. Sci. Instrum.*, 1958, **29**, 688–691.

43 S. Braun, H. -O. Kalinowski and S. Berger, *150 and More Basic NMR Experiments: a practical course*, WILEY-VCH, Weinheim, 1998, ch. 6.2.

44 H. Maki, K. Ibaragi, Y. Fujimoto, H. Nariai and M. Mizuhata, *Colloids Surf. A*, 2015, **484**, 153–163.

Tables

Table 1. Fitting parameters of the linear approximating for the relationships between the integrated intensities per FID scan (I_{freeAl}) of ^{27}Al NMR signals due to free $[Al(H_2O)_6]^{3+}$ ion in *x* mol L^{-1} $Al(NO_3)_3$ + 0.1 mol L^{-1} HNO_3 aq. (*x* = ca. 1 × 10^{-4} – 1 mol L^{-1}) at 30 °C and the $[Al(H_2O)_6]^{3+}$ concentrations as shown in Fig. 1(a) and 1(b). All raw data are listed in Table S1(Supporting Information).

(a) Linearly approximating for the real number axis plot (Fig. 1(a)) by eqn 1.

Slope	Intercept	Correlation coefficient
1.691×10^3	-3.70×10^3	0.99978

(b) Linearly approximating for the logarithmic axis plot (Fig. 1(b)) by eqn 2.

Slope	Intercept	Correlation coefficient
0.99617	3.223	0.99945

Table 2. Fitting parameters of the linear approximating for the NMR measurement parameter dependences of the integrated intensities per FID scan (I_{freeAl}) of ^{27}Al NMR signals due to $[Al(H_2O)_6]^{3+}$ ion in 0.1 mol L^{-1} $Al(NO_3)_3$ + 0.1 mol L^{-1} HNO_3 aq. at 30 °C as shown in Fig. 2(a) and 2(b). All raw data are listed in Table S2(Supporting Information).

(a) Number of FID scans dependence

Slope	Intercept	Correlation coefficient
1.661×10^5	1.847×10^5	1.0000

(b) Receiver gain dependence

Slope	Intercept	Correlation coefficient
0.0497	1.738×10^5	0.99996

Table 3. Temperature dependence of the fitting parameters of the linear approximating by eqn 2 for the logarithmic axis plot between the integrated intensities per FID scan (I_{freeAl}) of ^{27}Al NMR signals due to $[Al(H_2O)_6]^{3+}$ ion in *x* mol L^{-1} $Al(NO_3)_3$ + 0.1 mol L^{-1} HNO_3 aq. (*x* = ca. 1 – 1000 mmol L^{-1}) and the Al^{3+} concentrations as shown in Fig. 3(a), 3(b), and 3(c). All raw data are listed in Table S3(Supporting Information).

Temperature (°C)	Slope	Intercept	Correlation coefficient
21.4	1.0068	3.219	0.99989
30.0	1.0029	3.217	0.99991
40.0	0.9981	3.203	0.99985

Figure captions

Fig. 1. Relationships between the integrated intensity per FID scan (I_{freeAl}) of ^{27}Al NMR signals due to $[Al(H_2O)_6]^{3+}$ ion in *x* mol L^{-1} $Al(NO_3)_3$ + 0.1 mol L^{-1} HNO_3 aq. (*x* = ca. 0.1 – 1000 mmol L^{-1}) at 30 °C and $[Al(H_2O)_6]^{3+}$ concentrations. (a) double linear chart, (b) double logarithmic chart. Solid lines refer to the calculated straight lines by the use of pertinent parameters in Table 1 obtained by the linear approximation. The I_{freeAl} values are converted into the values before the input into the RF amplifier in an NMR spectrometer (i.e., corresponding to the receiver gain of 0 dB). All raw data are listed in Table S1(Supporting Information).

Fig. 2. NMR measurement parameter dependence of the integrated intensities of ^{27}Al NMR signals due to $[Al(H_2O)_6]^{3+}$ ion in 0.1 mol L^{-1} $Al(NO_3)_3$ + 0.1 mol L^{-1} HNO_3 aq. at 30 °C. NMR measurement parameter: (a) number of FID scans, (b) receiver gain of a RF amplifier, (c) FID acquisition time. The integrated intensities for (b) and (c) are the values per FID scan, and for (a) and (c) are converted into the values before the input into the RF amplifier in an NMR spectrometer (i.e., corresponding to the receiver gain of 0 dB). Solid lines refer to the calculated straight lines by the use of pertinent parameters in Table 2 obtained by the linear approximation. All raw data are listed in Table S2(Supporting Information).

Fig. 3. Effect of the sample solution temperature on the relationships between the integrated intensities per FID scan (I_{freeAl}) of ^{27}Al NMR signals due to $[Al(H_2O)_6]^{3+}$ ion in *x* mol L^{-1} $Al(NO_3)_3$ + 0.1 mol L^{-1} HNO_3 aq. (*x* = ca. 1 – 1000 mmol L^{-1}) and the $[Al(H_2O)_6]^{3+}$ concentrations. Temperature of sample solution: (a) 21.4 °C (i.e., room temperature), (b) 30 °C, (c) 40 °C. Solid lines refer to the calculated straight lines by the use of pertinent parameters in Table 3 obtained by the linear approximation. The I_{freeAl} values are converted into the values before the input into the RF amplifier in an NMR

spectrometer (i.e., corresponding to the receiver gain of 0 dB). All raw data are listed in Table S3(Supporting Information).

Fig. 4. Stack plot for the concentration ratio of OH/Al (0 < OH/Al < 9) dependence of ^{27}Al NMR spectra of PAC aqueous solutions after aging for 1 week at 30 °C. Total concentration of aluminum: (a) 10 mmol L^{-1}, (b) 50 mmol L^{-1}, (c) 100 mmol L^{-1}.

Fig. 5. OH/Al dependences of the total aluminum concentration distribution in generated various aluminum complexes in PAC aqueous solutions after aging for 1 week at 30 °C. Variation of pH (top), calculated from ^{27}Al qNMR (middle) and calculated from traditional Ferron assay (bottom). Total concentration of aluminum: (a) 10 mmol L^{-1}, (b) 50 mmol L^{-1}, (c) 100 mmol L^{-1}.

Fig. 6. Aging time dependences of the sample solution pH and the total aluminum concentration distribution in various hydrolyzed species of Al which were calculated from ^{27}Al qNMR of PAC aqueous solutions at 30 °C. Total concentration of aluminum: (top) 50 mmol L^{-1}, (bottom) 100 mmol L^{-1}. Concentration ratio of OH/Al: (a) 1, (b) 2, (c) 3.5. The abbreviations of “d”, “wk”, and “mo” denote “day”, “week”, and “month”, respectively.

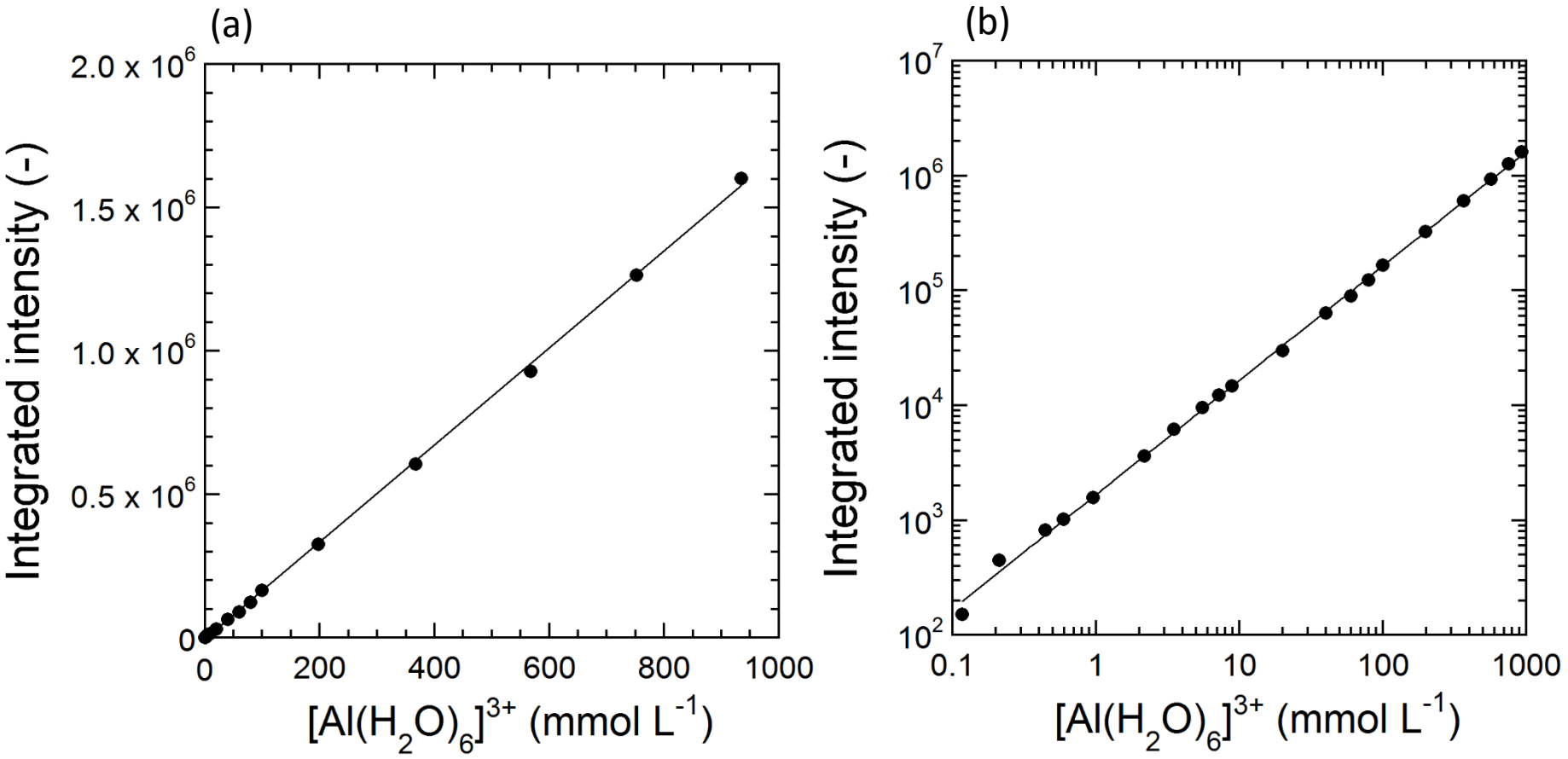
(a)
Integrated intensity (-)
2.0 x 10^6
1.5 x 10^6
1.0 x 10^6
0.5 x 10^6
0
0
200
400
600
800
1000
[Al(H2O)6]3+ (mmol L-1)
(b)
Integrated intensity (-)
10^7
10^6
10^5
10^4
10^3
10^2
0.1
1
10
100
1000
[Al(H2O)6]3+ (mmol L-1)

Figure 1

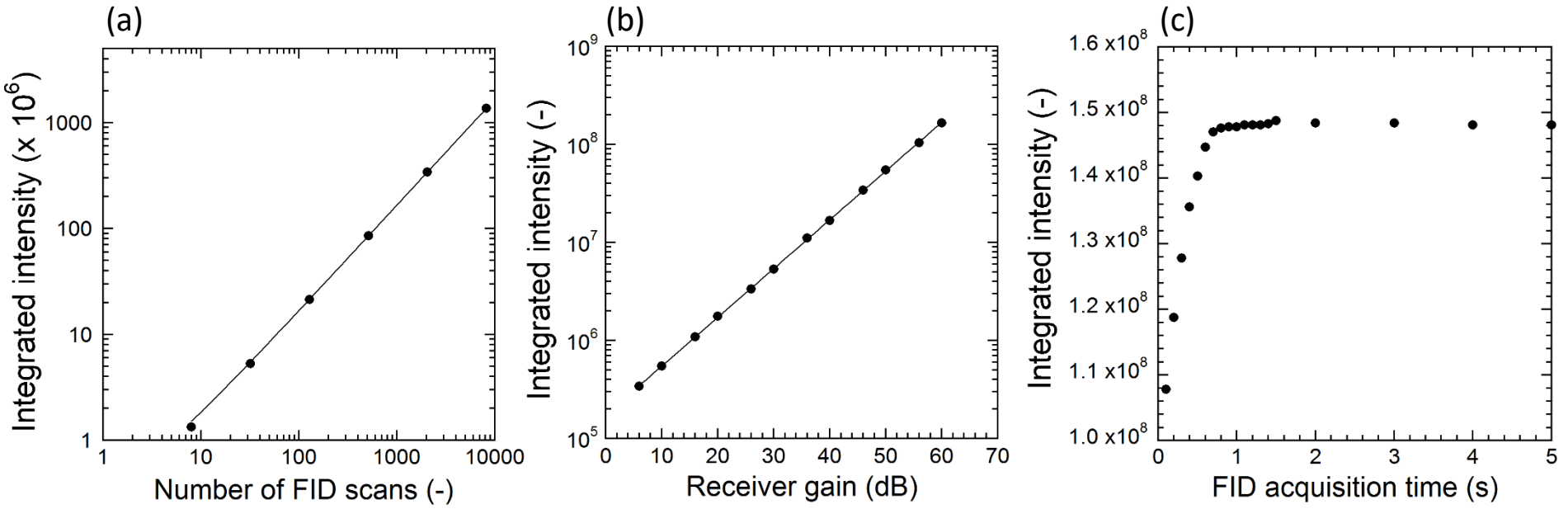
(a)
Integrated intensity (x 10^6)
1000
100
10
1
1
10
100
1000
10000
Number of FID scans (-)
(b)
Integrated intensity (-)
10^9
10^8
10^7
10^6
10^5
0
10
20
30
40
50
60
70
Receiver gain (dB)
(c)
Integrated intensity (-)
1.6 x10^8
1.5 x10^8
1.4 x10^8
1.3 x10^8
1.2 x10^8
1.1 x10^8
1.0 x10^8
0
1
2
3
4
5
FID acquisition time (s)

Figure 2

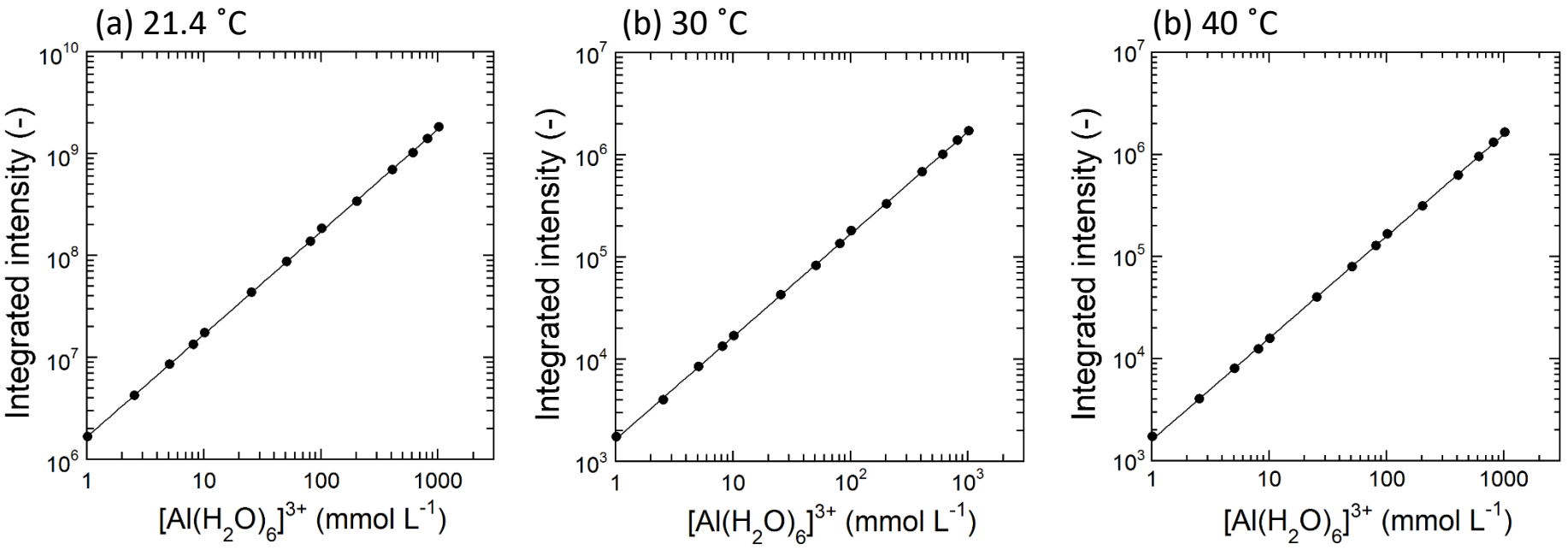

Figure 3

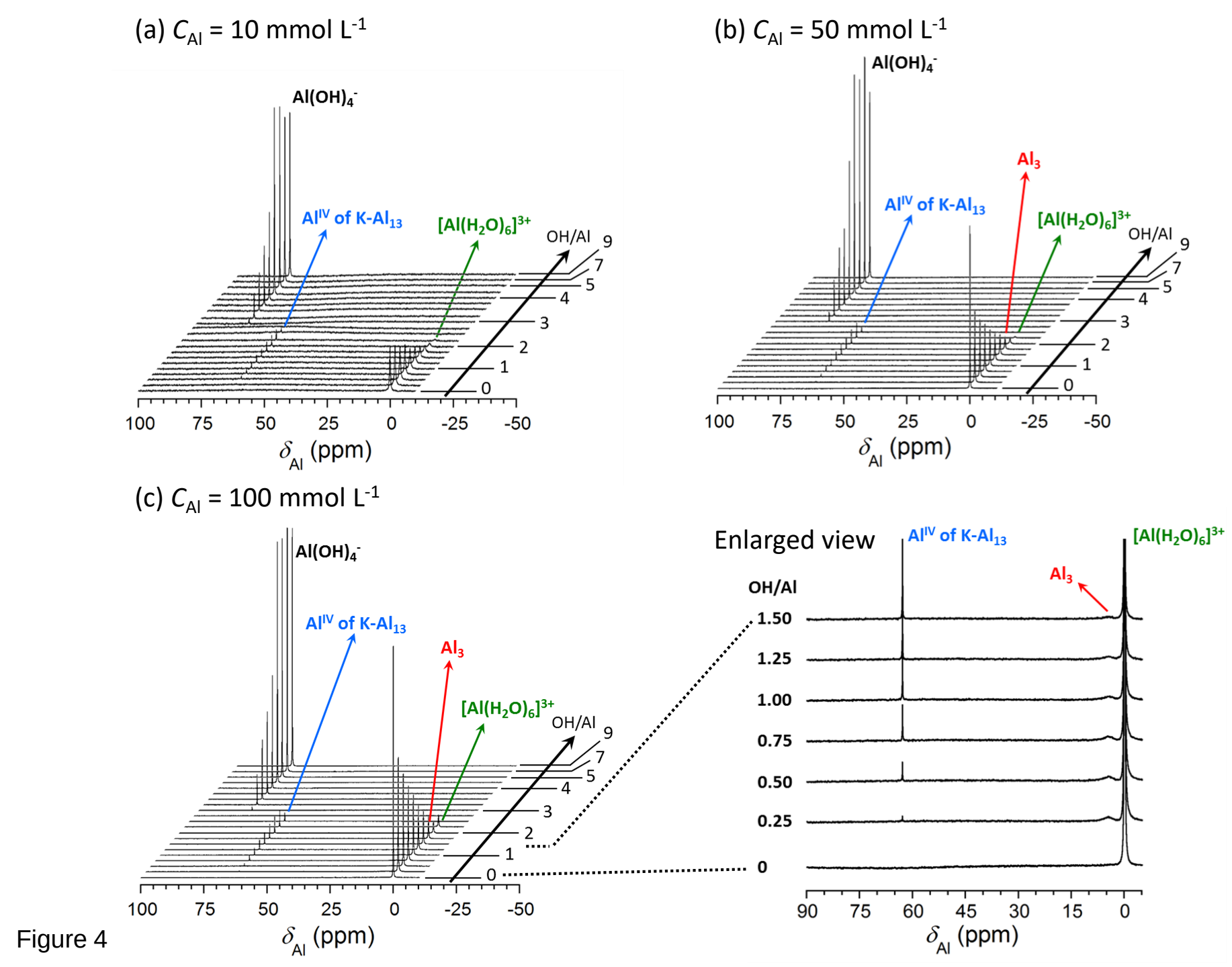
(a) C_{Al} = 10 mmol L^{-1}
$Al(OH)_4^-$
Al^{IV} of K-Al_{13}
$[Al(H_2O)_6]^{3+}$
OH/Al
9
7
5
4
3
2
1
0
100 75 50 25 0 -25 -50
δ_{Al} (ppm)
(b) C_{Al} = 50 mmol L^{-1}
$Al(OH)_4^-$
Al_3
Al^{IV} of K-Al_{13}
$[Al(H_2O)_6]^{3+}$
OH/Al
9
7
5
4
3
2
1
0
100 75 50 25 0 -25 -50
δ_{Al} (ppm)
(c) C_{Al} = 100 mmol L^{-1}
$Al(OH)_4^-$
Al^{IV} of K-Al_{13}
Al_3
$[Al(H_2O)_6]^{3+}$
OH/Al
9
7
5
4
3
2
1
0
100 75 50 25 0 -25 -50
δ_{Al} (ppm)
Enlarged view
Al^{IV} of K-Al_{13}
$[Al(H_2O)_6]^{3+}$
Al_3
OH/Al
1.50
1.25
1.00
0.75
0.50
0.25
0
90 75 60 45 30 15 0
δ_{Al} (ppm)

Figure 4

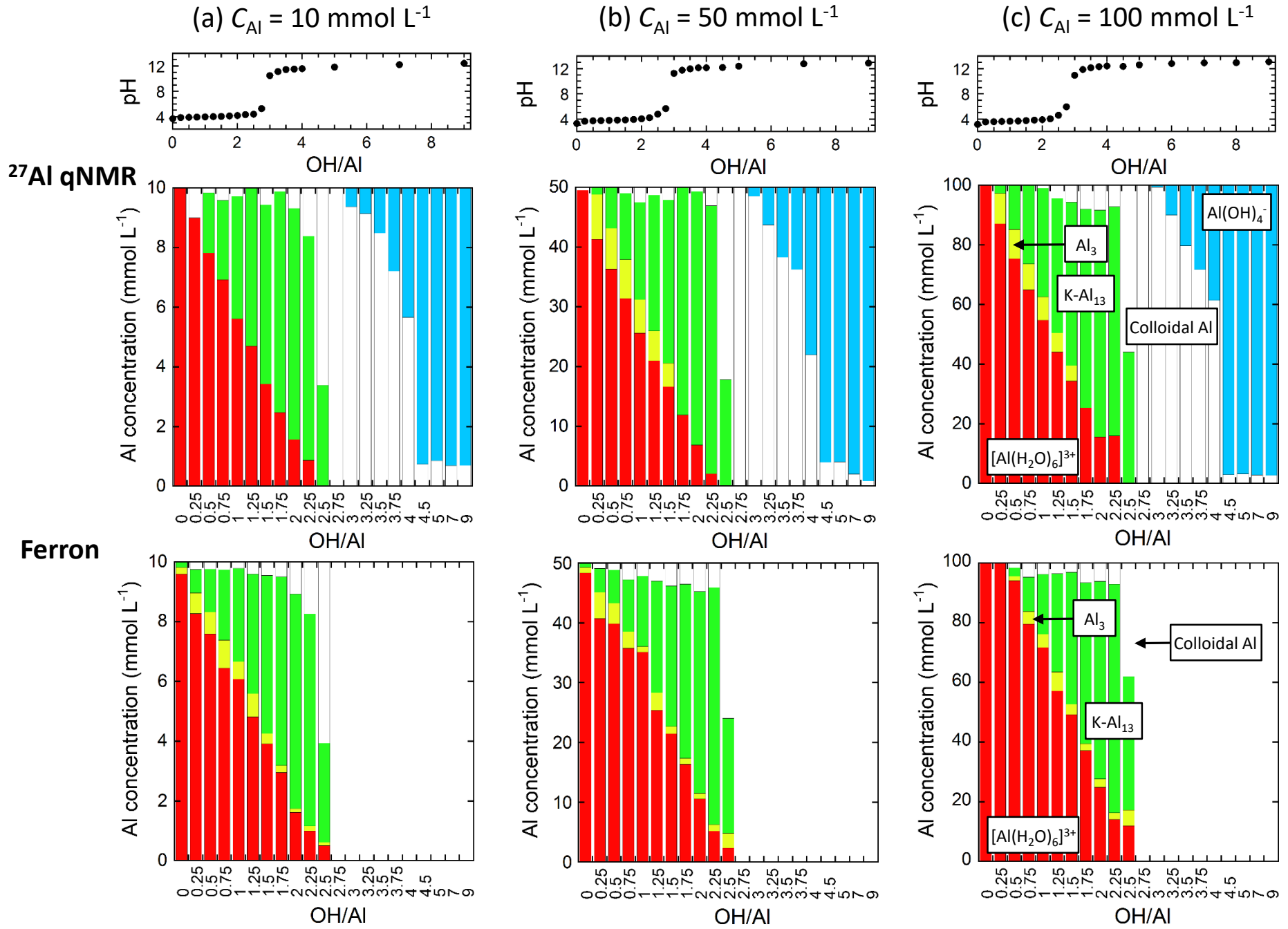
(a) C_{Al} = 10 mmol L^{-1}
(b) C_{Al} = 50 mmol L^{-1}
(c) C_{Al} = 100 mmol L^{-1}
pH
OH/Al
^{27}Al qNMR
Ferron
Al concentration (mmol L^{-1})
Al_3
K-Al_{13}
Colloidal Al
$Al(OH)_4^-$
$[Al(H_2O)_6]^{3+}$

Figure 5

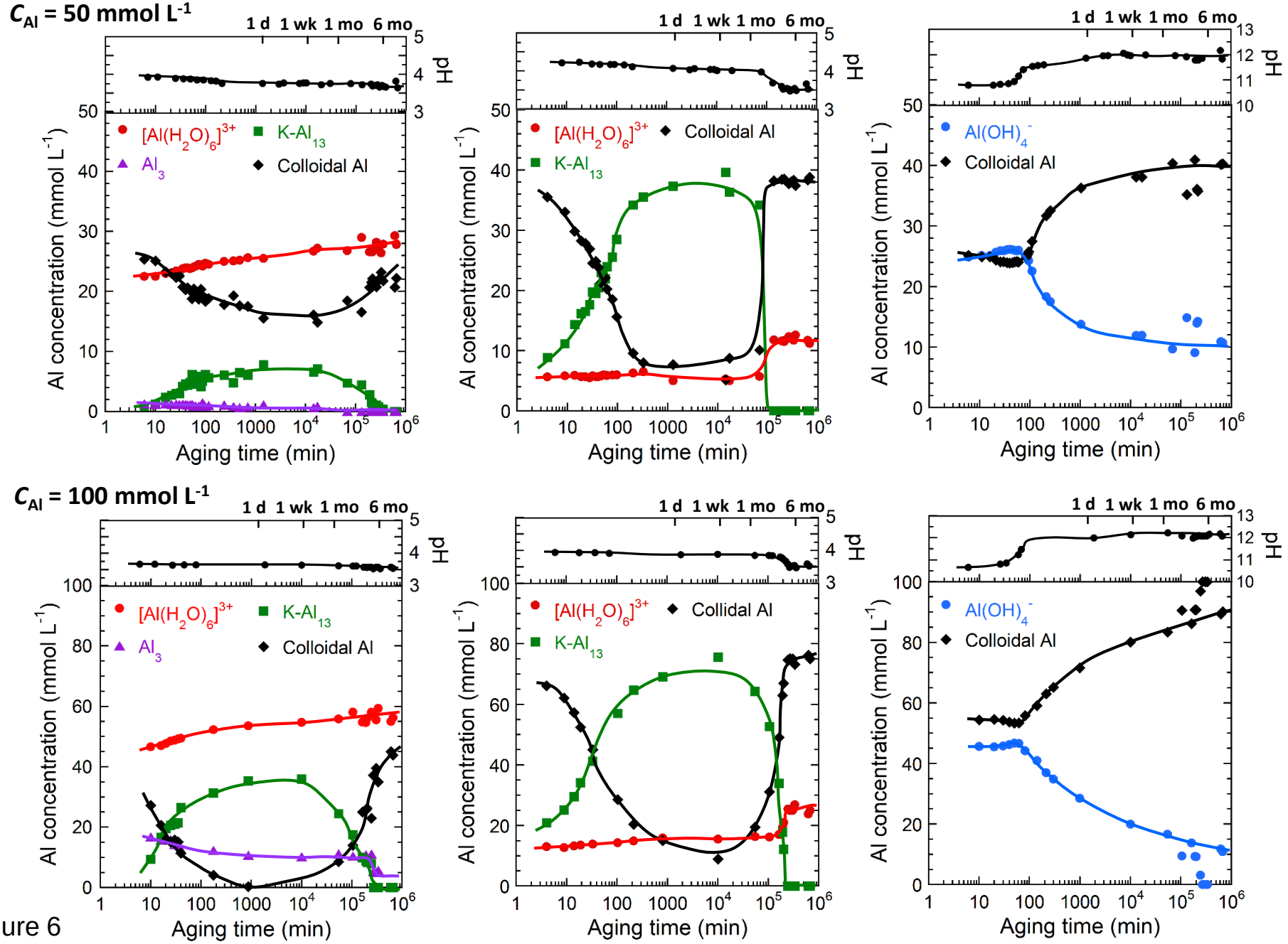
(a) OH/Al = 1
(b) OH/Al = 2
(c) OH/Al = 3.5
C_{Al} = 50 mmol L^{-1}
C_{Al} = 100 mmol L^{-1}
1 d 1 wk 1 mo 6 mo
pH
Al concentration (mmol L^{-1})
Aging time (min)
$[Al(H_2O)_6]^{3+}$
Al_3
K-Al_{13}
Colloidal Al
Collidal Al
$Al(OH)_4^-$

Figure 6

Supporting Information

Quantitative NMR of quadrupolar nucleus as a novel analytical method : Hydrolysis behavior analysis of aluminum ion

Hideshi Maki[a,b]*, Genki Sakata[b], Minoru Mizuhata[b]

[a]Center for Environmental Management, Kobe University, 1-1 Rokkodai-cho, Nada-ku, Kobe 657-8501, Japan

[b]Department of Chemical Science and Engineering, Graduate School of Engineering, Kobe University, 1-1 Rokkodai-cho, Nada-ku, Kobe 657-8501, Japan

*Corresponding author: maki@kobe-u.ac.jp

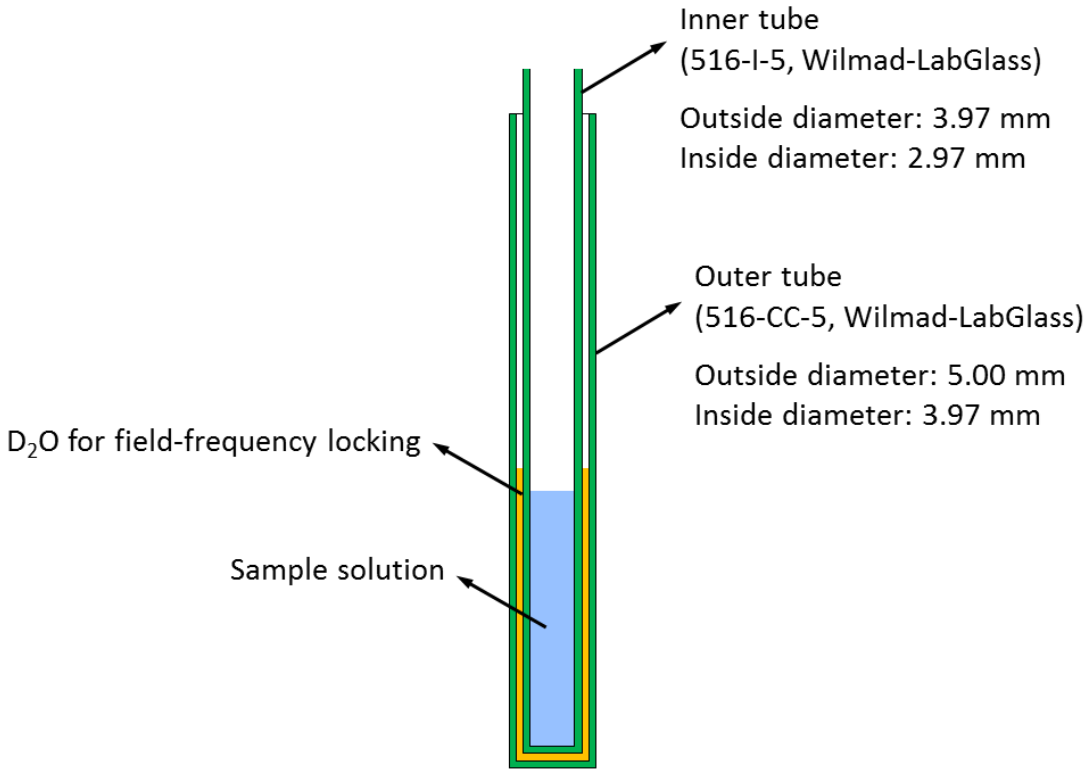

Scheme S1. Coaxial NMR tube system to avoid the contamination of D_2O for field-frequency locking into the sample solutions.

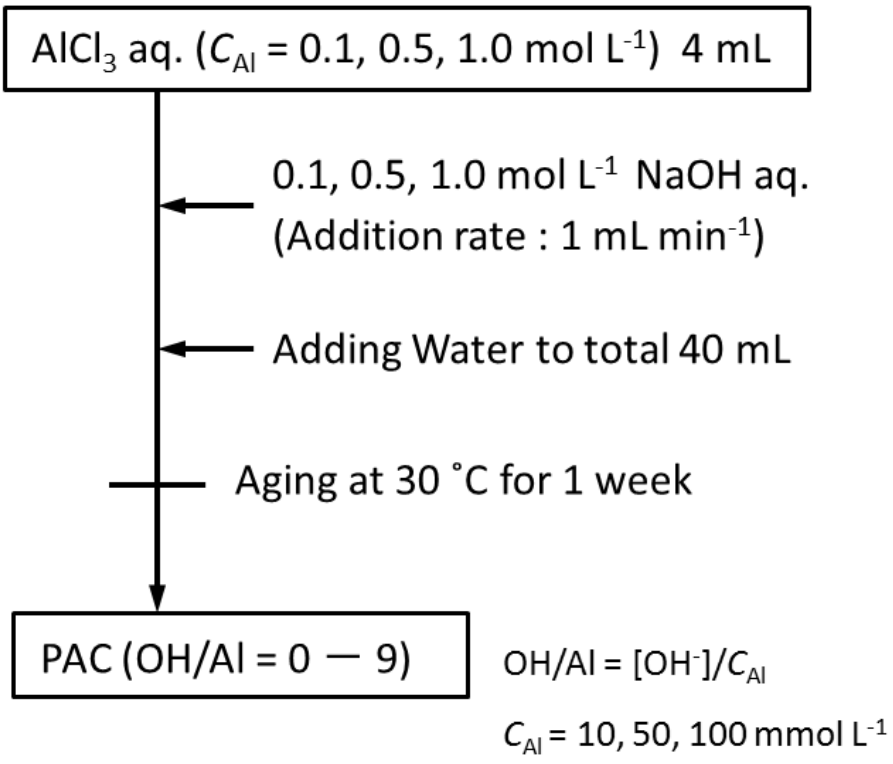

Scheme S2. Preparation of PAC sample solutions.

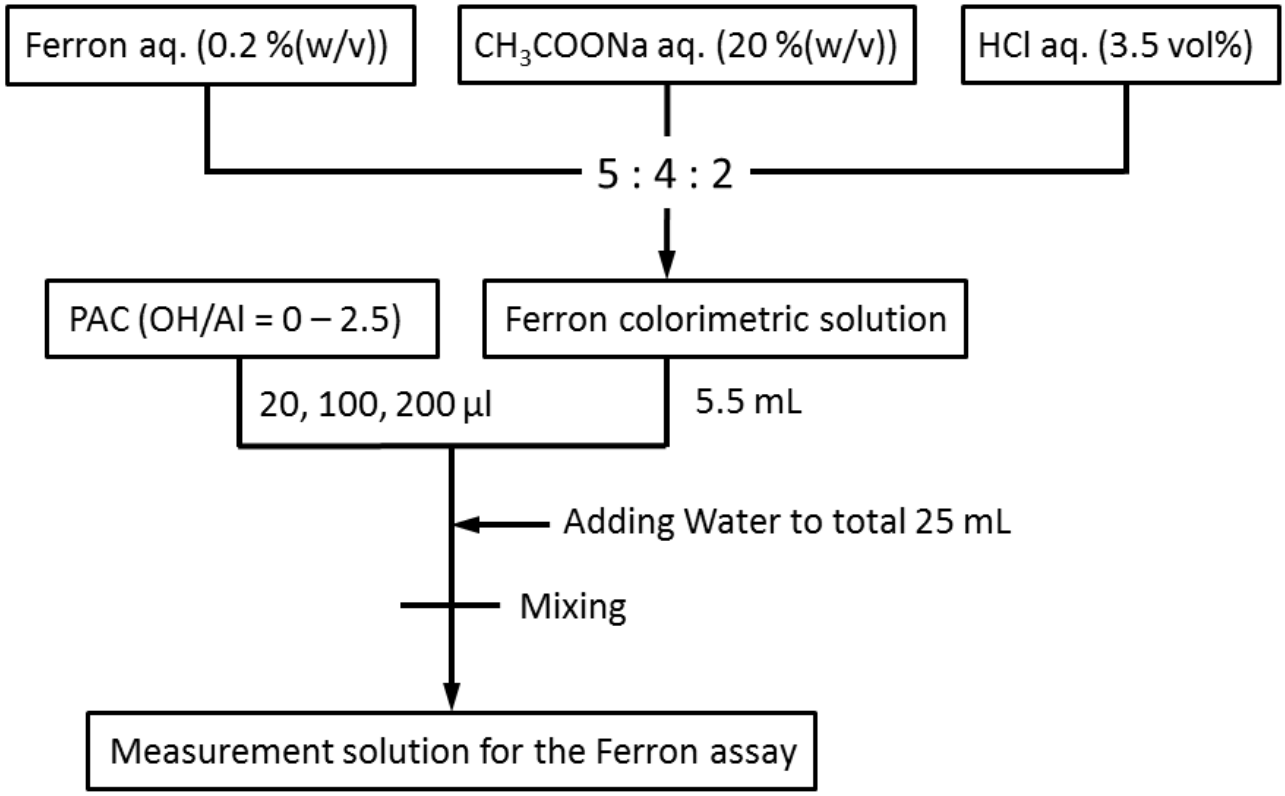

Scheme S3. Preparation of measurement solution for the Ferron assay.

Table S1. All raw data for the relationships between the integrated intensities per FID scan (I_{freeAl}) of ^{27}Al NMR signals due to $[Al(H_2O)_6]^{3+}$ ion in x molL^{-1} $Al(NO_3)_3$ + 0.1 molL^{-1} HNO_3 aq. (x = ca. 0.1 – 1 mol L^{-1}) at 30 °C and the $[Al(H_2O)_6]^{3+}$ concentrations (C_{freeAl}) as shown in Figs. 1(a) and 1(b). The I_{freeAl} values are converted into the values before the input into the RF amplifier in an NMR spectrometer (i.e., corresponding to the receiver gain of 0 dB).

C_{freeAl} (mmolL^{-1})	log (C_{freeAl}) (mmolL^{-1})	I_{freeAl}	log (I_{freeAl})
0.1173	-0.931	1.512×10^2	2.18
0.212	-0.673	4.49×10^2	2.65
0.446	-0.351	8.16×10^2	2.91
0.594	-0.226	1.015×10^3	3.01
0.959	-0.01800	1.571×10^3	3.20
2.19	0.340	3.60×10^3	3.56
3.51	0.546	6.17×10^3	3.79
5.55	0.744	9.53×10^3	3.98
7.20	0.858	1.236×10^4	4.09
8.85	0.947	1.475×10^4	4.17
20.0	1.301	3.01×10^4	4.48
40.0	1.602	6.38×10^4	4.80
60.0	1.778	8.99×10^4	4.95
80.0	1.903	1.232×10^5	5.09
100.0	2.00	1.656×10^5	5.22
197.7	2.30	3.26×10^5	5.51
368	2.57	6.05×10^5	5.78
568	2.75	9.30×10^5	5.97
752	2.88	1.265×10^6	6.10
935	2.97	1.602×10^6	6.20

Table S2. All raw data for the NMR measurement parameter dependences of the integrated intensities of ^{27}Al NMR signal (I_{freeAl}) due to $[Al(H_2O)_6]^{3+}$ ion ion in 0.1 mol L^{-1} $Al(NO_3)_3$ + 0.1 mol L^{-1} HNO_3 aq. at 30 °C as shown in Figs. 2(a) and 2(b). The I_{freeAl} values for Fig. 2(a) are converted into the values before the input into the RF amplifier in an NMR spectrometer (i.e., corresponding to the receiver gain of 0 dB). The integrated intensities for Fig. 2(b) are the values per FID scan.

(a) Number of FID scans dependence

Number of FID scans	I_{freeAl}
8	1.335×10^6
32	5.31×10^6
128	2.13×10^7
512	8.54×10^7
2048	3.41×10^8
8192	1.361×10^9

(b) Receiver gain dependence

Receiver gain (dB)	I_{freeAl}
6	3.42×10^5
10	5.46×10^5
16	1.084×10^6
20	1.763×10^6
26	3.35×10^6
30	5.32×10^6
36	1.111×10^7
40	1.671×10^7
46	3.41×10^7
50	5.48×10^7
56	1.041×10^8
60	1.660×10^8

Table S3. All raw data for the effect of the sample solution temperature on the relationships between the integrated intensities per FID scan of ^{27}Al NMR signals due to $[Al(H_2O)_6]^{3+}$ ion in x mol L^{-1} $Al(NO_3)_3$ + 0.1 mol L^{-1} HNO_3 aq. (x = ca. 1 – 1000 mmol L^{-1}) and the $[Al(H_2O)_6]^{3+}$ ion concentrations as shown in Figs. 3(a), 3(b), and 3(c). The I_{freeAl} values are converted into the values before the input into the RF amplifier in an NMR spectrometer (i.e., corresponding to the receiver gain of 0 dB).

(a) 21.4 °C (i.e., room temperature)

C_{reeAl} (mmol L^{-1})	log (C_{reeAl}) (mmol L^{-1})	I_{freeAl}	log (I_{freeAl})
1.020	0.00860	1.675×10^3	3.224
2.55	0.4065	4.26×10^3	3.629
5.10	0.7076	8.56×10^3	3.932
8.16	0.9117	1.340×10^4	4.127
10.20	1.0086	1.752×10^4	4.244
25.5	1.4065	4.36×10^4	4.640
51.0	1.7076	8.73×10^4	4.941
81.6	1.912	1.376×10^5	5.139
102.0	2.009	1.847×10^5	5.267
204	2.310	3.42×10^5	5.534
408	2.611	6.95×10^5	5.842
612	2.787	1.023×10^6	6.010
816	2.912	1.409×10^6	6.149
1020	3.009	1.829×10^6	6.262

(b) 30 °C

C_{reeAl} (mmol L^{-1})	log (C_{reeAl}) (mmol L^{-1})	I_{freeAl}	log (I_{freeAl})
1.020	0.00860	1.751×10^3	3.243
2.55	0.4065	4.00×10^3	3.602
5.10	0.7076	8.51×10^3	3.930
8.16	0.9117	1.337×10^4	4.126
10.20	1.0086	1.697×10^4	4.230
25.5	1.4065	4.29×10^4	4.632
51.0	1.7076	8.28×10^4	4.918
81.6	1.912	1.350×10^5	5.130
102.0	2.009	1.819×10^5	5.260
204	2.310	3.30×10^5	5.518
408	2.611	6.84×10^5	5.835
612	2.787	1.008×10^6	6.004
816	2.912	1.397×10^6	6.145
1020	3.009	1.718×10^6	6.235

(c) 40 °C

C_{reeAl} (mmol L^{-1})	log (C_{reeAl}) (mmol L^{-1})	I_{freeAl}	log (I_{freeAl})
1.020	0.00860	1.728×10^3	3.237
2.55	0.4065	4.05×10^3	3.608
5.10	0.7076	8.01×10^3	3.903
8.16	0.9117	1.244×10^4	4.095
10.20	1.0086	1.587×10^4	4.201
25.5	1.4065	4.03×10^4	4.606
51.0	1.7076	7.93×10^4	4.899
81.6	1.912	1.277×10^5	5.106
102.0	2.009	1.676×10^5	5.224
204	2.310	3.15×10^5	5.498
408	2.611	6.31×10^5	5.800
612	2.787	9.61×10^5	5.983
816	2.912	1.319×10^6	6.120
1020	3.009	1.649×10^6	6.217

Table S4. ^{27}Al spin-lattice and spin-spin relaxation times, i.e., T_1 and T_2, of all aluminum species were determined by the inversion recovery[40,41] and the CPMG procedure[42-44]. Total concentration of aluminum (C_{Al}) is 100 mmol L^{-1}.

Chemical shift	0 ppm	4.0 ppm	62.5 ppm	80 ppm
Species	$[Al(H_2O)_6]^{3+}$	Al_3	K-Al_{13}	$Al(OH)_4^-$
T_1 (s)	0.035*	0.0014*	0.040*	0.013**
T_2 (s)	0.028*	0.0015*	0.034*	0.011**

*Determined from the sample solution of OH/Al = 1.25

** Determined from the sample solution of OH/Al = 4.0

Table S5. Fitting parameters and reaction rate constant, k, which were derived from a nonlinear least squares curve fitting method by the Ferron assay of PAC aqueous solutions after aging for 1 week at 30 °C.

(a) C_{Al} = 10 mmol L^{-1}

OH/Al	A_0	A_∞	A_1	$A_2 (A_\infty - A_0)$	k_{b1}	k_{b2}	R
0	0.6195	0.6195	0.10407	0.08706	0.06992	0.0003217	0.94493
0.25	0.6038	0.6038	0.12627	0.14479	0.08261	0.0006955	0.98416
0.50	0.4211	0.6049	0.09437	0.18386	0.06458	0.0007862	0.99732
0.75	0.3575	0.6035	0.09765	0.2460	0.06689	0.0007310	0.99855
1.00	0.3369	0.6060	0.05104	0.2691	0.03981	0.0008570	0.99915
1.25	0.2672	0.5941	0.06389	0.3269	0.004192	0.0006971	0.99846
1.50	0.2174	0.5913	0.02435	0.3740	0.02190	0.0009467	0.99955
1.75	0.16400	0.5888	0.015752	0.4248	0.015287	0.0007925	0.99987
2.00	0.08985	0.5530	0.008229	0.4632	0.005048	0.0008749	0.99972
2.25	0.05528	0.5120	0.010663	0.4567	0.005728	0.0008047	0.99982
2.50	0.02796	0.2437	0.007243	0.2158	0.003333	0.0007019	0.99968

(b) C_{Al} = 50 mmol L^{-1}

OH/Al	A_0	A_∞	A_1	$A_2 (A_\infty - A_0)$	k_{b1}	k_{b2}	R
0	0.5307	0.6362	0.14077	0.10554	0.08851	0.0003644	0.88508
0.25	0.4467	0.6248	0.19666	0.17808	0.11930	0.0006671	0.95170
0.50	0.4375	0.6215	0.11327	0.18405	0.07564	0.0007569	0.99327
0.75	0.3926	0.6010	0.06683	0.2084	0.05035	0.0008850	0.99754
1.00	0.3853	0.6089	0.017868	0.2235	0.007634	0.0008993	0.99874
1.25	0.2785	0.5983	0.05081	0.3198	0.03886	0.0009583	0.99879
1.50	0.2358	0.5878	0.018443	0.3520	0.016507	0.0009977	0.99950
1.75	0.17947	0.5915	0.014217	0.4121	0.011904	0.0010337	0.99952
2.00	0.11594	0.5759	0.012572	0.4600	0.007566	0.0010691	0.99958
2.25	0.05709	0.5842	0.0144	0.5271	0.004990	0.0010608	0.99996
2.50	0.02796	0.2437	0.007243	0.2158	0.003333	0.0007019	0.99968

(c) C_{Al} = 100 mmol L^{-1}

OH/Al	A_0	A_∞	A_1	$A_2(A_\infty - A_0)$	k_{b1}	k_{b2}	R
0	0.5527	0.6409	0.10405	0.08824	0.07064	0.0004093	0.95192
0.25	0.5535	0.6284	0.06248	0.07483	0.04912	0.0004495	0.99029
0.50	0.4999	0.6307	0.06622	0.13078	0.04930	0.0007246	0.99605
0.75	0.4226	0.6104	0.06912	0.18782	0.05072	0.0008799	0.99638
1.00	0.3808	0.6170	0.05163	0.2362	0.03986	0.0009378	0.99704
1.25	0.3036	0.6182	0.06082	0.3147	0.04484	0.00092114	0.99846
1.50	0.2615	0.6212	0.02837	0.3598	0.02505	0.00099744	0.99924
1.75	0.19763	0.5985	0.016816	0.4009	0.014226	0.0010621	0.99935
2.00	0.13216	0.6018	0.019884	0.4696	0.013553	0.0010489	0.99925
2.25	0.07495	0.5951	0.01534	0.5202	0.006760	0.0010835	0.99951
2.50	0.06341	0.3969	0.03926	0.3335	0.02276	0.0008521	0.99620

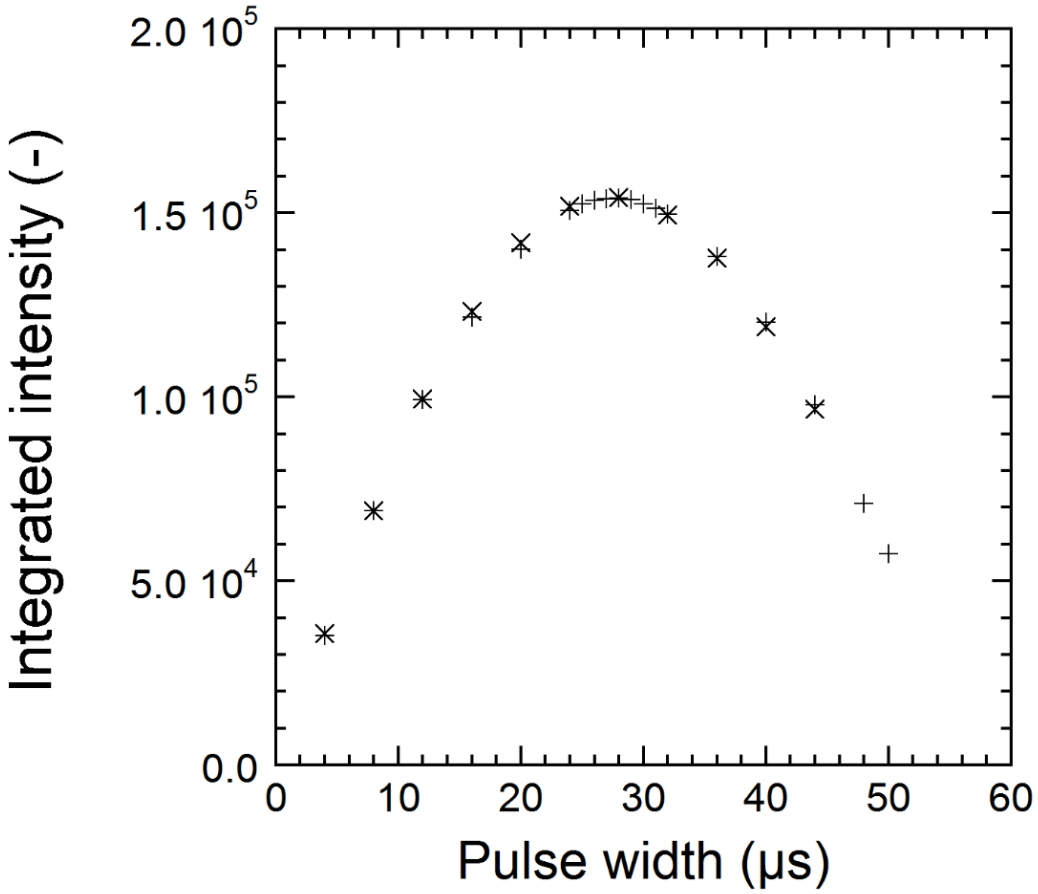

Fig. S1. Influence of anionic species on the pulse width dependence of the integrated intensities per FID scan (I_{freeAl}) of ^{27}Al NMR signals due to $[Al(H_2O)_6]^{3+}$ ion at 30 °C. The I_{freeAl} values are converted into the values before the input into the RF amplifier in an NMR spectrometer (i.e., corresponding to the receiver gain of 0 dB). Sample solution: (+) 0.1 mol L^{-1} $Al(NO_3)_3$ + 0.1 mol L^{-1} HNO_3, (×) 0.1 mol L^{-1} $AlCl_3$ + 0.1 mol L^{-1} HCl.

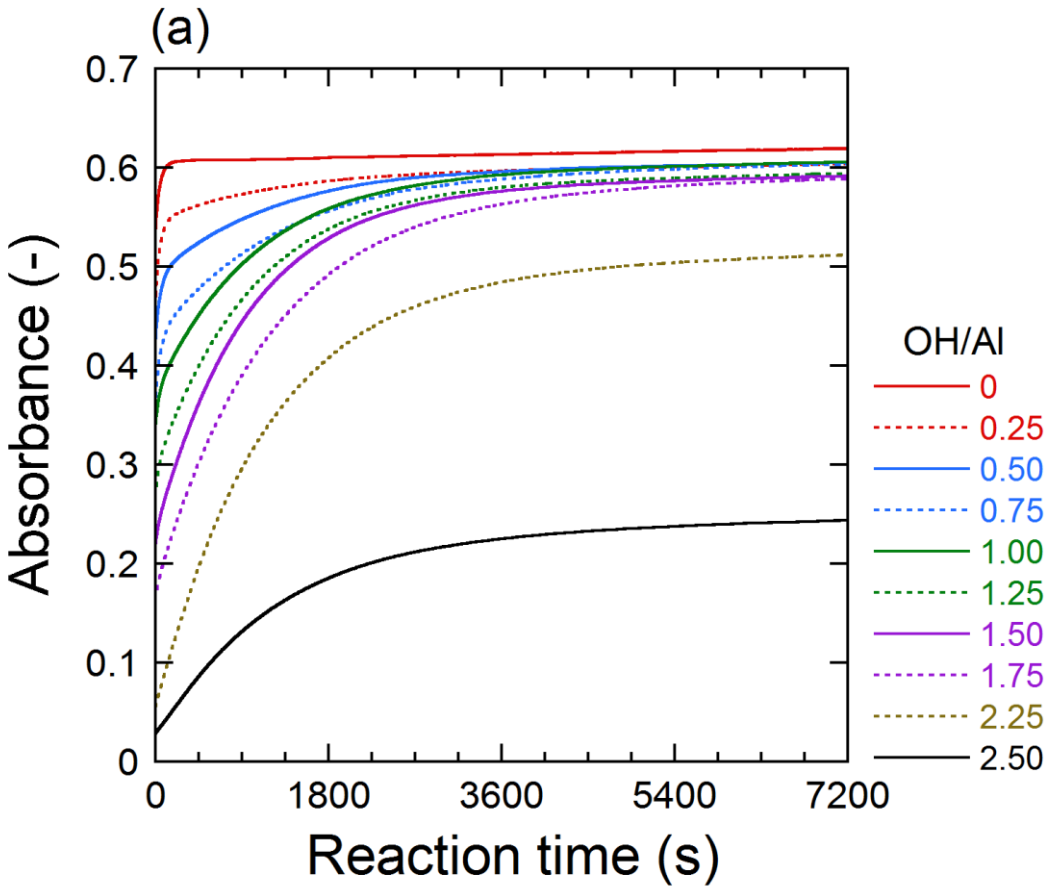
(a)
Absorbance (-)
0.7
0.6
0.5
0.4
0.3
0.2
0.1
0
0
1800
3600
5400
7200
Reaction time (s)
OH/Al
0
0.25
0.50
0.75
1.00
1.25
1.50
1.75
2.25
2.50

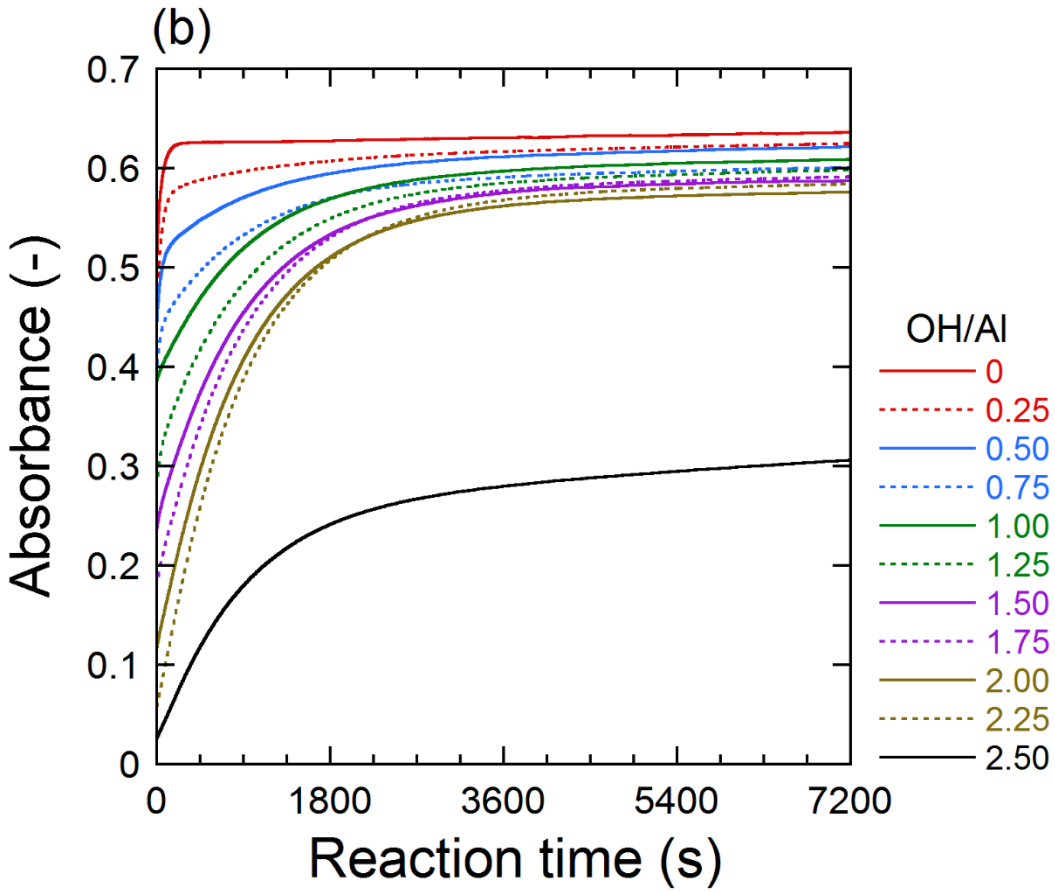
(b)
Absorbance (-)
0.7
0.6
0.5
0.4
0.3
0.2
0.1
0
0
1800
3600
5400
7200
Reaction time (s)
OH/Al
0
0.25
0.50
0.75
1.00
1.25
1.50
1.75
2.00
2.25
2.50

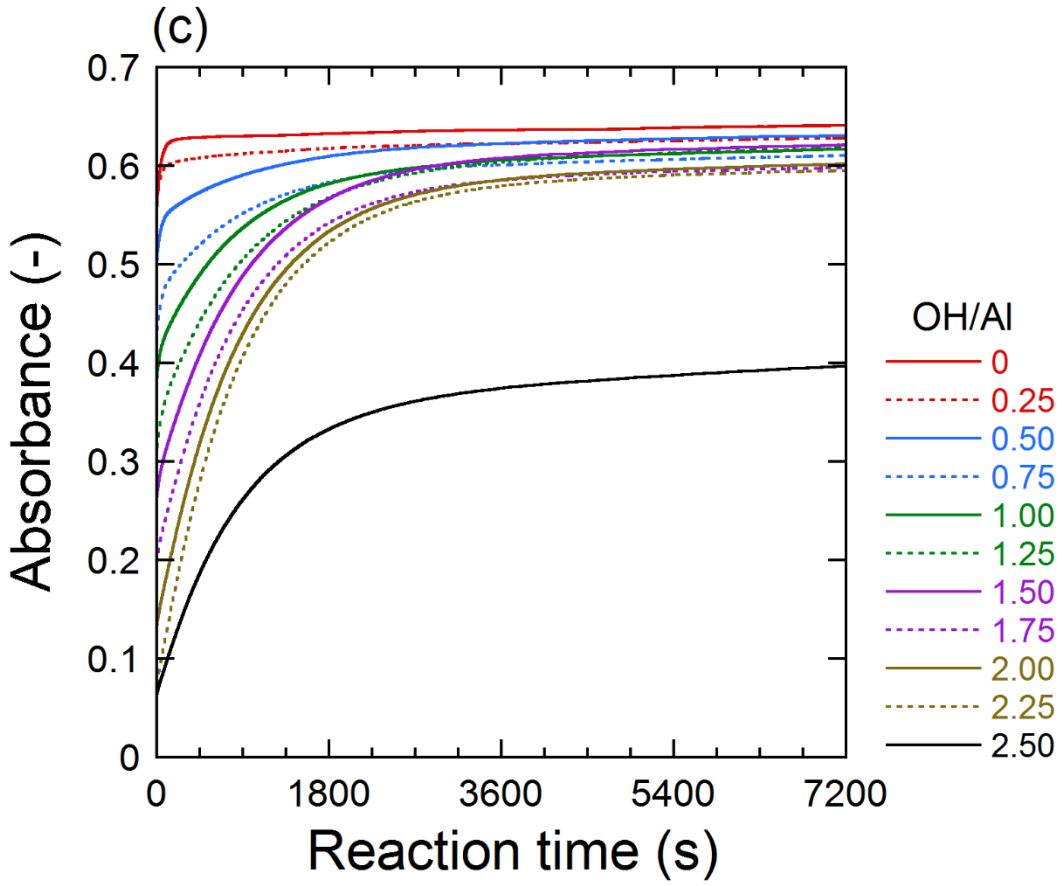

Fig. S2. Time course of absorbance for the Ferron assay of PAC aqueous solutions after aging for 1 week at 30 °C. Total concentration of aluminum: (a) 10 mmol L^{-1}, (b) 50 mmol L^{-1}, (c) 100 mmol L^{-1}.